Strojniški vestnik - Journal of Mechanical Engineering 59(2013)3, 139-147

DOI:10.5545/sv-jme.2012.483

Received for review: 2012-03-16
Received revised form: 2012-05-11
Accepted for publication: 2012-05-16

3D Numerical Analysis of 2D Profile Bending with the Torque Superposed Spatial Bending Method

Matej Hudovernik[1,*] – Daniel Staupendahl[2] – Mohammad Gharbi[2] – Matthias Hermes[2] – A. Erman Tekkaya[2] – Karl Kuzman[3] – Janez Marko Slabe[1]

[1]Tecos, Slovenian Tool and Die Development Centre, Slovenia
[2]Institute of Forming Technology and Lightweight Construction (IUL), Germany
Technische Universität Dortmund, Germany
[3]University of Ljubljana, Faculty of Mechanical Engineering, Slovenia

Engineering research, in the field of light weight design, is strongly oriented towards the development of new high strength materials and innovative forming methods, capable of withstanding limitations with regard to the wide variety of technological and economical aspects. Cost effective lightweight construction, in addition to the reduction of energy/material consumption and overall reduction of weight, also strongly depends on stability, continuity and robustness of production processes. Kinematic solutions for the production of spatial designed structures, in terms of 3D bending of profiles and tubes, show great potential in an increase of efficiency in the field of light weight design. The Torque Superposed Spatial bending method - TSS, developed at the Institute of Forming Technology and Lightweight Construction, Technische Universität Dortmund, represents an innovative, robust and cost effective technical solution for 2D and 3D bending of tubes and profiles and offers a wide spectrum of capabilities, such as process continuity, parameter adaptation and flexibility for spatial bending of profiles with arbitrary cross-sections. In this paper, an introduction to 3D numerical analysis of the 2D profile bending method using TSS method is introduced and presented. The first objective of the work is to establish validity of the numerical model for the bending parameters, such as the bending force and bending momentum. Secondly, further investigations of the state of stresses and strains during load and unload conditions were performed. These are important for any further analysis and understanding of spring-back, residual stresses and cross section deformation of the profiles. The numerical simulations are performed with the use Abaqus software code, with elastic plastic material characteristics, and are, for the purpose of validation, compared to experimental data.

Keywords: TSS, Torque Superposed Spatial, 3D FEM analysis, 2D profile bending, numerical simulations

0 INTRODUCTION

Demands for efficient, lightweight, and spatial designed components and parts are nowadays growing rapidly. Decrease of material consumption and an overall reduction of weight are the main reasons for the development of new high strength materials and robust, flexible, and cost effective engineering solutions for the cold forming of tubes and profiles [1] and [2]. Especially three-dimensionally bent profiles show a great potential in an increase of part efficiency by providing optimal material distribution, a reduction of number of parts, and thereby a decrease of assembly procedures.

The need for profile parts with complex 3D contours represents a demanding challenge for any conventional manufacturing method (i.e. [2] to [4]). Existing innovative solutions (i.e. [5] to [9]) for the production of such spatial profile and tubular components show the importance of and the necessity for robust and adaptive manufacturing techniques. Studies regarding TSS bending method have shown its vast potential in forming of profiles made of high strength steels (i.e. [10] to [13]). The TSS bending method offers a great number of advantages such as the increase of process efficiency by decreasing the number of manufacturing steps, and a decrease of production time [10] and [12]. The process parameters, such as bending force and bending momentum, and forming phenomena occurring during the process of bending with a variable bending radius, have not been studied in detail by numerical methods yet. Therefore, computer aided numerical simulations play an essential role in the understanding of the TSS bending method. The existence of complex states of stresses during processing can be analyzed in detail after validation of the bending force and bending momentum parameters. The 3D numerical analysis of TSS profile bending process is given using implicit software code of Abaqus/standard. Results of the simulations were analyzed and validated with experimental data.

1 TSS PROFILE BENDING METHOD

The basic mechanical principles of bending with the TSS bending method, are in many ways similar to those of conventional bending technologies. Unwanted phenomena as tearing, necking, lateral buckling and wrinkling are likely to develop during the bending

*Corr. Author's Address: TECOS, Kidričeva 25, 3000 Celje, Slovenia, matej.hudovernik@tecos.si

process, if input parameters are not consistent with material characteristics and cross-section properties [14]. Geometrical accuracy, material properties, spring-back, and residual stresses strongly depend on process stability and must be controlled specifically in order to get sufficient results and a high overall product quality [1].

Conventional technologies show many disadvantages regarding the prediction of forming behavior and the overall product quality (i.e. [15] to [20]. The kinematic TSS bending method offers an innovative approach to solving tasks of bending high strength steel profiles by operating in three parallel phases: continuous profile transportation, plasticization during bending, and the application of torque that is needed to perform the change of plane position and realization of 3D geometry.

The basic graphic scheme of the TSS bending process is shown in Fig. 1. The operational functionality of the TSS bending method is built upon the feed of the profile along the c axis with a constant or variable velocity by clamping the profile and pushing it forward by rotation of 6 roll based system. The 2D bending of the profile is realized by the pre-defined numerically controlled movement of the bending head along the x axis, positioned perpendicular to the transportation axis c. The 3D bending contour is accomplished by superposing a torque onto the plane bending process. This is achieved by the numerically controlled rotation of the torsion bearing (α_1), mounted around the feeding mechanism. This event causes the change of the bending plane position relative to the profile and creates a 3D shaped contour, as shown in Fig. 1. The two compensation axes (α_2- and τ-axis) of the bending head self-align themselves during the process according to the movement of the profile to achieve a tangential run of the bending head relative to the profile [11] and [21].

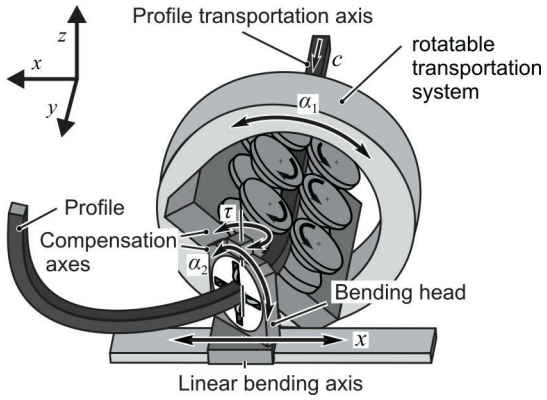

Fig. 1. *Graphic scheme for TSS bending method [10]*

2 PROCESS ANALYSIS

The analysis of 2D and 3D bending of profiles using TSS bending method can be built upon analytical formulations for the bending of tubes and beams with different sections, as presented and described in (i.e. [14] and [21] to 24]). The parameters of the TSS bending process can later be predicted for each individual input material by the use of finite element methods. Spring-back, cross-section deformations, residual stresses, and material properties can therefore be evaluated by using appropriate software code and by comparison with experimental data.

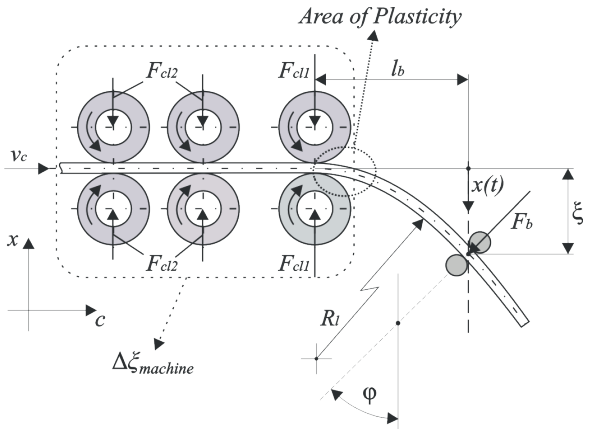

Fig. 2. *TSS bending mechanism*

El Megharbel et al. [14], describe analytical techniques to determine the bending moment, for 2D bending of square hollow profile cross-section (Fig. 3), and work hardening elastic-plastic material properties. Similarly, this can be applied to the TSS bending method.

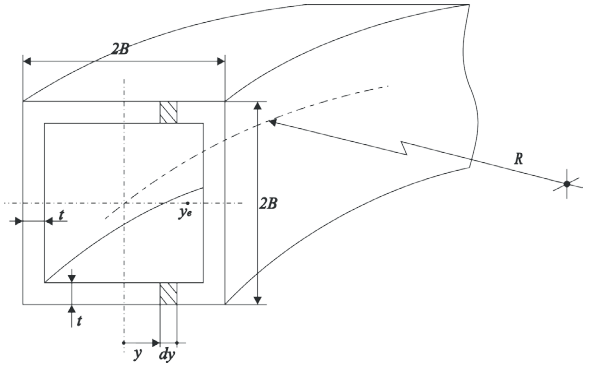

Fig. 3. *Hollow cross section of the profile [14]*

It is assumed, that the yield point y_e is located with the definition of $y_e \leq B - t$ [14]. Stress-strain relationship in the field of elastic plastic properties is defined with [14]:

$$\sigma_{el} = E \cdot \varepsilon \quad \text{for} \quad \varepsilon \leq \varepsilon_y , \tag{1}$$

$$\sigma_{pl} = C \cdot \varepsilon_n \quad \text{for} \quad \varepsilon \geq \varepsilon_y , \tag{2}$$

$$\varepsilon = y / R . \tag{3}$$

These analytical principals are used as the basis for the development of the numerical analysis.

3 MATERIALS AND METHODS

All numerical and experimental investigations are based on a 40×40×2.5 mm profile made from air hardening MW1000L Z3 high strength steel [25]. According to the manufacturer, the yield strength of MW1000L is measured at 900 MPa, and the tensile strength at 1100 MPa [24]. The behaviour of this material can be compared to 15CrMoV6 steel, but offers a 14 to 20% higher breaking elongation [25].

The flow curve for MW1000L Z3 high strength steel was described using standard tensile tests and the (Eq. (4)). The flow curve for this specific high strength steel is shown in Fig. 4.

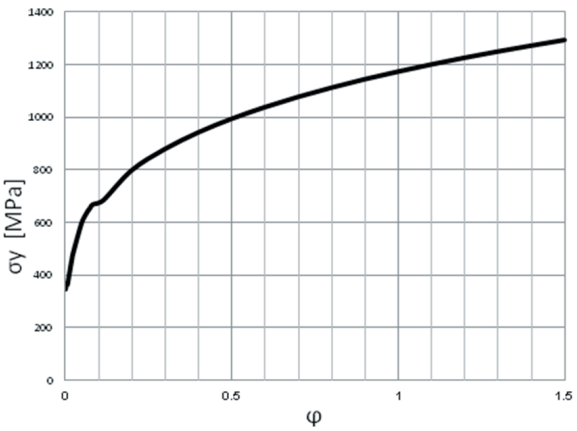

Fig. 4. *Flow curve for MW1000L Z3 high strength steel*

Table 1. *Material properties for MW1000L steel [25]*

v	E [GPa]	G [GPa]	$R_{p0.2}$ [MPa]	R_m [MPa]
0.3	200	80	900	1100

The target profile contour for the analysis is shown in Fig. 5. An experimental analysis for the TSS bending process limits using this contour is shown by Staupendahl et al. [12]. The 2D profile bending target contour incorporates variable bending radii ranging from r_{min} = 400 mm, to r_{max} = 2000 mm and thus offers the possibility to study a wide range of radii using a single profile shape. To achieve a continuous curvature in the numerical and experimental analyses, the single radii were replaced by a continuous spline producing an effective radius trend of 1985 to 416 mm.

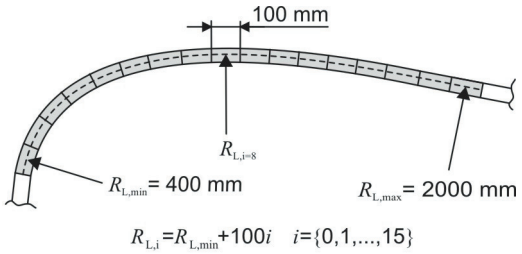

Fig. 5. *Investigated profile contour*

To generate the axes movements that are necessary to produce the target curvature, digital mock-ups were used (Fig. 6). The mock-up was setup using the kinematics module of CATIA V5 (Dessault Systems). As the profile is fed through the mock-up at a constant velocity, the x-axis and τ-axis movements are generated accordingly.

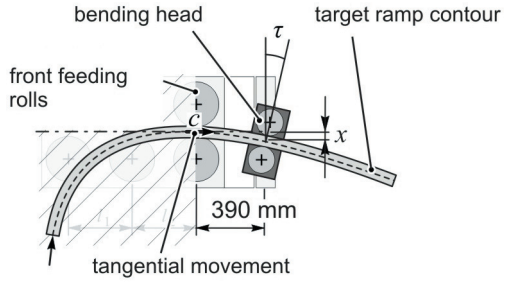

Fig. 6. *Setup of TSS bending mock-up to generate axes movements [12]*

4 NUMERICAL SIMULATION SETTINGS

The numerical model for 2D profile bending was tested with the use of implicit Abaqus software code. The Von Mises yield criteria and isotropic material work hardening rule were assigned to the model.

All tools – the feeding rolls, and bending head – were defined as analytically rigid elements. Influences of elasticity of tools were not considered within the described test model, but these important factors are to be considered in the future research.

4.1 Mesh Properties

The numerical model was tested with the use of Abaqus/standard software code. The meshing of the FEM model was performed with the use of quadratic S8R – 8-node doubly curved thick shell elements – with reduced integration. The section was determined

with the Gauss integration rule and 5 integration points over the 2.5 mm thickness of the shell. For an optimal calculation time, approximately 5000 quad shell elements over the surface were evenly distributed.

4.2 Constraints and Loads

The bending head of an actual TSS machine consists of 4 rolls. This enables a sufficient transportation support for each outer side of the square profile cross-section. The bending head - in an actual TSS process constantly adapts its position with regard to the local curvature by free rotation around the vertical axis. The centre of this adaptive vertical rotation is always positioned on x axis according to the pre-defined NC program, and the bending head is always positioned tangential to the local profile curvature as shown in Fig. 7a. For the numerical simulation of 2D profile bending, the bending head is replaced with one single roll as shown in Fig. 7b. The movement is adjusted accordingly.

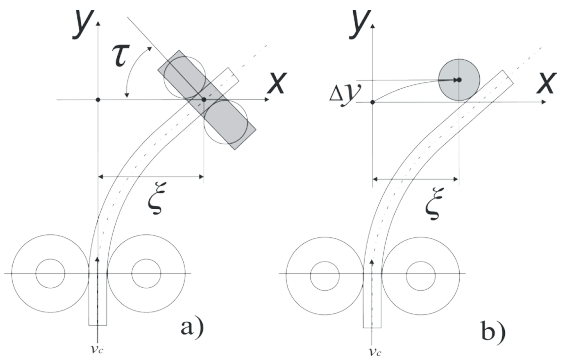

Fig. 7. *Replacement of 4 roll bending head with a single bending roll*

The FEM model for 2D profile bending using Abaqus/standard code is shown in Fig. 6.

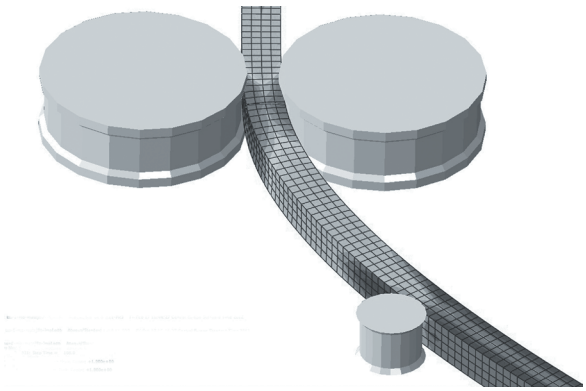

Fig. 8. *FEM model for 2D bending of profile using single bending roll*

The loads and boundary conditions are applied with specific amplitude settings by using the displacement/rotation and velocity/angular-velocity functions. The feed rolls are assigned with a constant angular velocity. The bending is applied by the movement of bending roll, as function of time and amplitude as shown in Fig. 9.

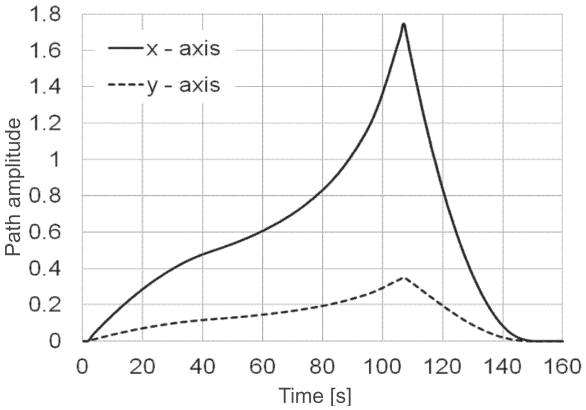

Fig. 9. *Amplitude functions for bending roll*

4.3 Contact Relations and Step Definition

Contact relations between the deformable body, meaning the profile, and all of the analytically rigid bodies such as the bending roll and the set of feeding rolls were set to prevent objects from penetrating each other. In an Abaqus implicit code, contact relationship between shell elements and analytic rigid bodies, are defined with surface to surface discretization method, penalty friction formulation in tangential domain and hard contact in normal behaviour domain. Friction coefficient μ was set to 0.3 concerning contact between feed rolls and shell elements, while frictionless characteristics were assigned to the relation between bending roll and profile.

The dynamic implicit steps, a full Newton solution technique allowing maximum of 10^6 number of increments and initial increment size of 10^{-5}, were defined.

5 EXPERIMENTAL ANALYSES

The experimental 2D bending of 40×40×2.5 mm profile, made of MW1000L steel, was performed by using the TSS bending machine setup shown in Fig. 10.

During the bending process, the x-component of the bending force was measured using a load cell integrated into the x-axis of the machine. With the

knowledge of the τ-axis rotation generated with the digital mock-up, the y-component of the bending force, as well as the actual bending force were calculated

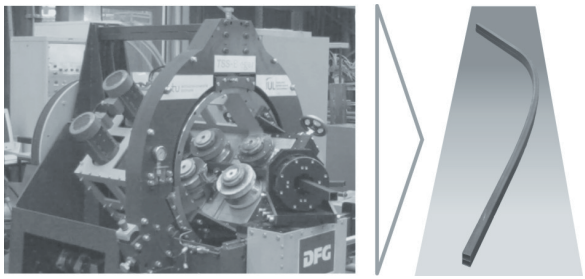

Fig. 10. *Experimental results of 2D profile bending using TSS bending method*

The contour deviations of the profiles were measured using the GOM Atos 3D scanning system. The best-fit measurement method showed a maximum offset of 0.60 mm. 90% of the profile actually lie in a spectrum of ±0.3 mm.

6 RESULTS

The FEM model for the analysis of 2D profile bending, defined with 5000 evenly distributed quadratic S8R shell elements, and a reduced integration technique was created in Abaqus standard implicit code. The overall calculation time for a numerical simulation was 23.6 hours.

The experimental analysis was oriented towards the test of repeatibility regarding geometrical accuracy of final product and validation of input parameters, such as bending forces F_{bx} and F_{by}, which were meassured during the process. By using these results, the resultant force F_b and the bending momentum M_b, were determined. The FEM model was validated by comparing the values of bending force and bending moment, which were calculated as a reaction to the movement of analyticaly rigid bending roll. Similar validation of parameters is presented in [26] and [27]. The comparison of experimental and numerical results, for the bending force components in relationship to feed of the profile and the original NC input data, are shown in Figs. 11 and 12. The comparison of the numerical and experimental values of the bending moment M_b, with regard to the feed of the profile and the original NC input data is presented in Fig. 13.

The values of numerically calculated force components, compared to experimental data, are slightly higher on the x axis. At approximately 1400 mm of the profile feed, the numerical value of F_{bx} reaches around 14 kN, while the value of the actual force in x direction is slightly lower, around 13.2 kN. The force slightly decreases at the point of 1600 mm profile feed, where the bending moment is at its maximum value, due to the plasticization of the material of the profile.

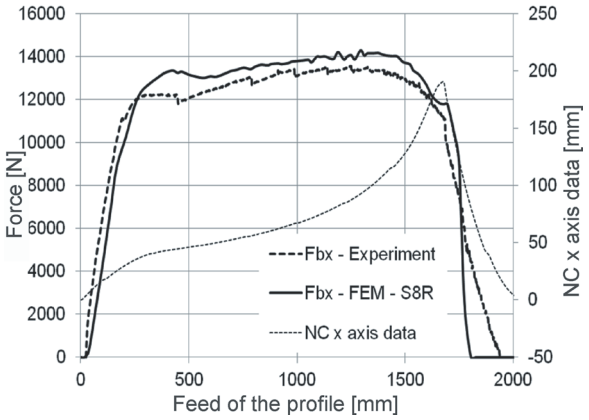

Fig. 11. *Comparison of bending force component in x axis F_{bx}*

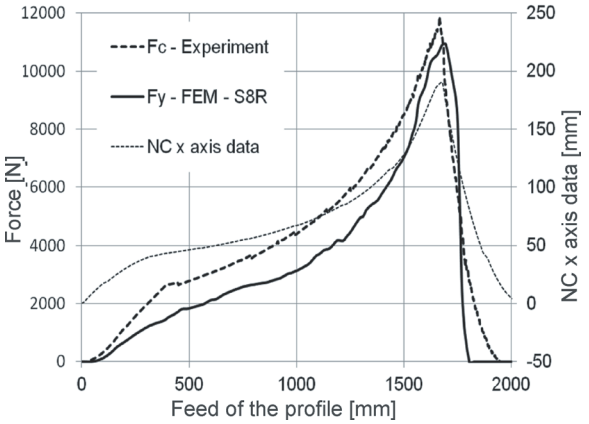

Fig. 12. *Comparison of bending force component in c axis F_{bc}*

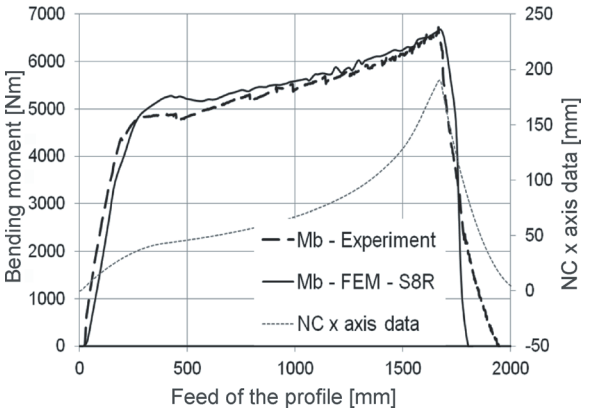

Fig. 13. *Comparison of the bending moment M_b*

The numerical results for F_{by}, which are shown in Fig. 12, are slightly lower than the actual data, but sufficiently approximate. The accuracy and consistency of bending moment results are shown and compared in Fig. 13.

The FEM model was validated, by bending force and bending momentum, with sufficient approximation to experimental data. Additional analysis procedures were, therefore, undertaken for 2D bending of square profile in order to understand the state of strains and stresses during bending in the profile material.

Results considering stress-strain relationship and related phenomena such as cross section deformations are presented in the following.

The material of the profile tends to plastify in the area shown in Fig. 14, during the application of bending load. In order to gain detailed understanding of how this affects the geometrical change of the profile cross-section, the work was oriented mainly to this specific area, at the time of maximum bending moment value. In this particular area of interest, the relationship between tensile and compressive stresses were analysed as shown in Fig. 15. The approximate position of neutral stress zone could, therefore, be evaluated.

The forming mechanism for the kinematic TSS 2D bending of square profile, with the specific input NC data, is charachterized by a larger compressive zone over the cross-section surface.

Detailed state of stresses in contrast to the plastic strain equivalent - PEEQ, over the cross-section width, are shown and described in Fig. 16a and b.

Fig. 16a shows the position of elements - el. 1 to 4 across the profile width, for which the stresses and PEEQ's were calculated and determined, with an average value of stresses and plastic strain equivalent, for the integration points. Numerical results presented in Fig. 16b, show the state of stresses and strains with regard to the conditions mentioned above. The

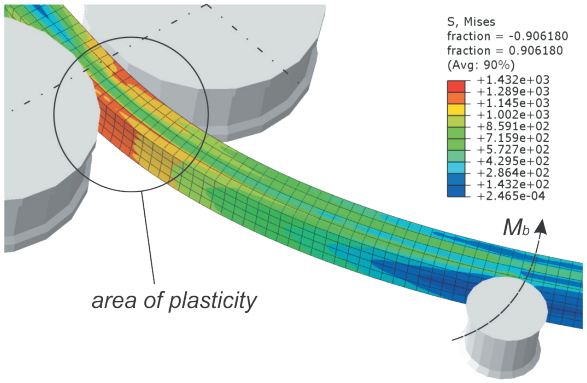

Fig. 14. *Area of plasticity for 2D profile bending*

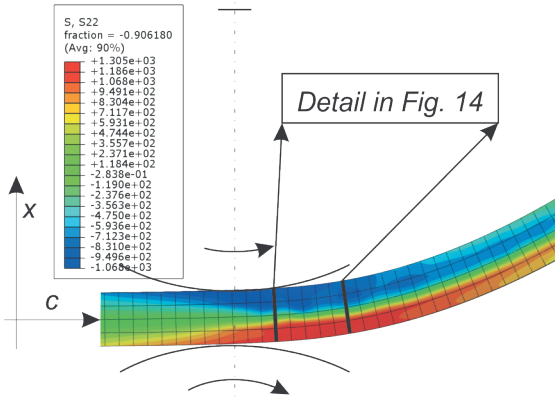

Fig. 15. *Tensile/compressive state of stresses in the area of plasticity*

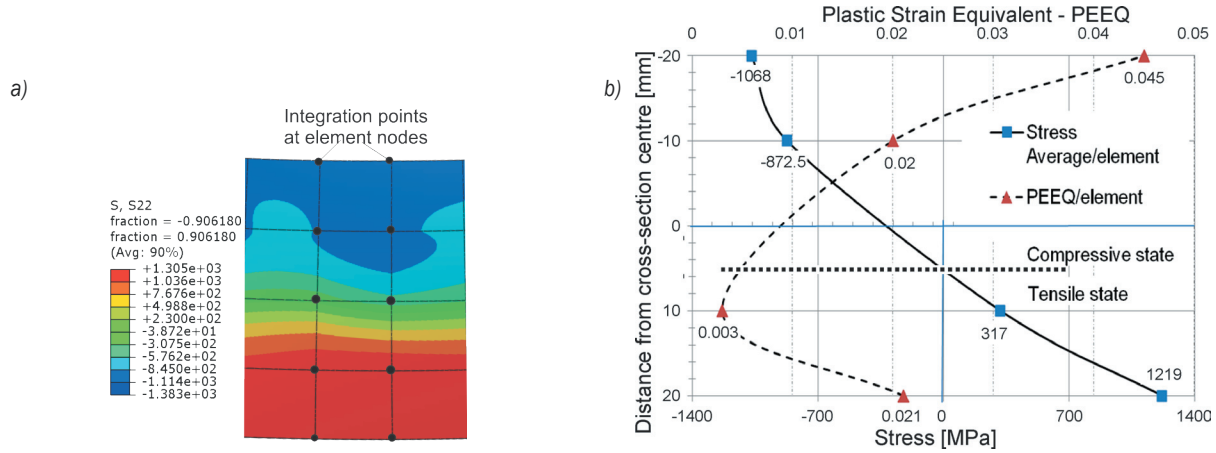

Fig. 16. *State of stresses and plastic strain equivalent at element node integration points for the detailed area described in Fig. 15*

horizontal doted line marks the position of neutral-stress zone, between tensile and compressive fields.

In the field of tensile stresses, these range up to 1200 MPa, while the PEEQ ranges from 0.021; at the points on the most outer contour, and down to around 0.003; at the points closer to the neutral zone. In the compressive zone, the PEEQ ranges up to 0.045, while stresses range down to –1068 MPa. The forming mechanism is, herefore, from this specific aspect, determined with a smaller tensile field, but higher stresses, compared to the compressive state, where stresses reach lower values, but plastic strains dominate the domain.

The bending load can also directly influence the vertical geometrical properties of the profile cross-section, marked in Fig. 17, which shows the cut of square profile cross-section in the area of plasticity (i.e. Fig. 15).

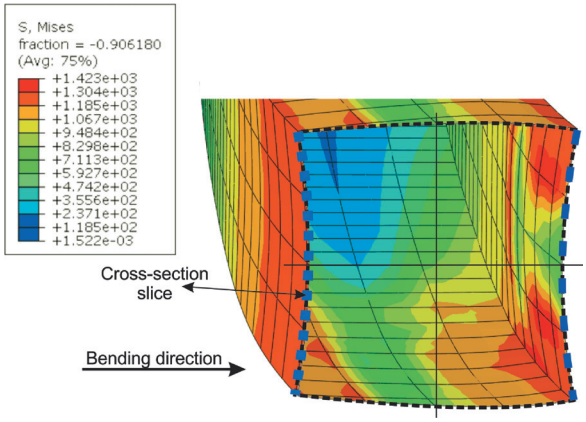

Fig. 17. *The profile slice used for analysis of cross-section deformation*

Fig. 17 presents the deformed state of the cross-section, and the average values of the Von Mises stress over the shell surface of the cross-section. In the tensile field – the outer vertical side of the cross-section – the average value of Von Mises stress amounts to approximately 1100 MPa. In the compressed field – the inner vertical side of the cross-section – this parameter averages to the slightly higher value of around 1200 Mpa.

The state of stresses after unloading, due to the unpredictible spring-back effect, are also presented in Fig. 18. This phenomena shows the substantial change in stress orientation.

During unloading, the previously compressive stresses in the inner vertical side of the cross-section, transform into tensile stresses, while those on the outer vertical side, transform into compressive. The stresses after unloading are, however, higher on the inner vertical side, with average values of approximately 500 MPa, while stresses on the outer side, range at negative values of around 200 MPa.

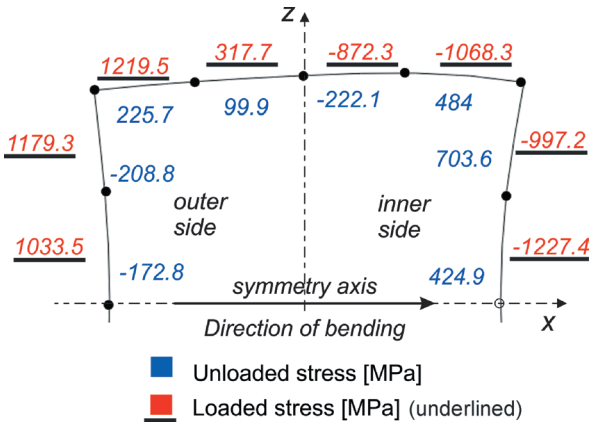

Fig. 18. *The state of stresses over cross-section area for loading and unloading conditions*

The state of the unloaded stresses in the upper and lower horizontal side of the cross-section also perform changes, which are not identical to inner and outer sides of the cross-section. The substantial change occurs only in the upper/lower right corner of the cross-section. The significant value of compressive stress there – 1068.3 MPa – transforms into tensile after unloading with a value of 484 MPa. The condition in the other horizontal elements, remain the same with the difference of decrease of stress values. The average PEEQ values, per each element in the cross-section, are presented in Fig. 19. As mentioned earlier, the values for plastic strain equivalents are higher in the compressive zone, ranging up to 0.045 on the horizontal side and up to 0.051 in the vertical inner side of the profile. The plastic strain values on the tensile side range up to 0.021 – on the horizontal, and up to 0.039 on the outer vertical side.

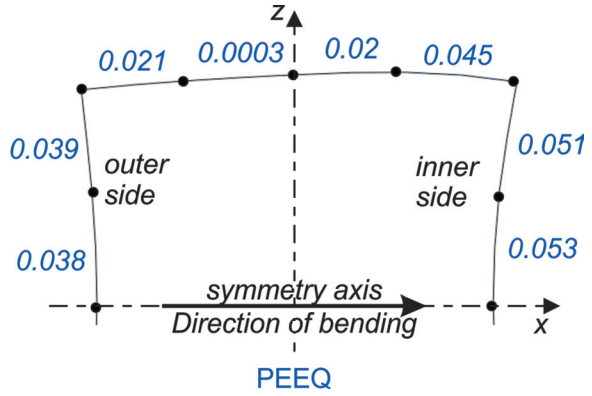

Fig. 19. *PEEQ over cross-section area*

Due to geometrical symmetry of the cross-section, only the upper half of the cross-section is presented. This specific subject of complex phenomena will also be an important part in the future of numerical research of the TSS bending method.

7 CONCLUSIONS

A 3D numerical analysis for 2D bending of square profiles with the TSS – torque superposed spatial – bending method, for the continued spline, defined with a variable bending radius, has been shown and presented in this paper. A numerical model was developed with the use of Abaqus/standard implicit software code. High strength material characteristics, as well as quadratic - S8R, doubly curved thick shell elements, and the Gauss integration rule with 5 integration points over the 2.5 mm thickness of the shell were assigned to the model. The overall time for the simulation was approximately 24 h.

The model was validated by comparison of numerical and experimental results, as shown in Figs. 11 to 13. Due to sufficient approximation of numerical results, regarding the focus on validating the bending force and the bending momentum parameters, in relation to the actual data, additional analysis regarding the state of stresses and strains in the area of plasticity and profile cross-section deformations, were performed. The shown results, represent the foreground for further work, regarding numerical analysis of 2D and 3D bending of symmetrical and asymmetrical profiles and the analysis of spring-back behaviour, the state of residual stresses, and the effect of elasticity of tools on the final profile contour.

8 ACKNOWLEDGEMENTS

The research leading to these results has received funding from the European Union's European Social Fund and from the European Union's Research Fund for Coal and Steel (RFCS) under grant agreement No. [RFSR-CT-2009-00017]. All experimental work was performed in close collaboration with the Institute of Forming Technology and Lightweight Construction - IUL, Technische Universität Dortmund.

9 REFERENCES

[1] Chatti, S. (2006). *Production of Profiles for Lightweight Structures*. Habilitation thesis, University of Franche-Comté, Books on Demand GmbH, Norderstedt.

[2] Kleiner, M., Chatti, S., Klaus, A. (2006). Metal forming techniques for lightweight construction. *Journal of Materials Processing Technology*, vol. 177, no. 2-7, p. 2-7, DOI:10.1016/j.jmatprotec.2006.04.085.

[3] Kleiner, M., Geiger, M., Klaus, A. (2003). Manufacturing of lightweight components by metal forming. *CIRP Annals – Manufacturing Technology*, vol. 52, no. 2, p. 521-542, DOI:10.1016/S0007-8506(07)60202-9.

[4] Jeswiet, J., Geiger, M., Engel, U., Kleiner, M., Schikorra, M., Duflou, J., Neugebauer, R., Bariani, P., Bruchi, S. (2008). Metal forming progress since 2000. *CIRP Journal of Manufacturing Science and Technology*, vol. 1, p. 2-17, DOI:10.1016/j.cirpj.2008.06.005.

[5] Goto, H., Ichiryu, K., Saito, H., Ishikura, Y., Tanaka, Y. (2008). Applications with a new 6-DOF bending machine in tube forming processes. *Proceedings of the 7th JFPS International Symposium on Fluid Power TOYAMA*, p. 15-18, DOI:10.5739/isfp.2008.183.

[6] Neugebauer, R., Drossel, W.G., Lorenz, U., Luetz, N. (2002). Hexabend - a new concept for 3D-free-form bending of tubes and profiles to preform hydroforming parts and space-frame-components. *Proceedings of the 7th ICTP Yokohama, vol. 2, Advanced Technology of Plasticity*, p. 1465-1470.

[7] Murata, M., Kuboti, T., Takahashi, K. (2007). Characteristics of tube bending by MOS bending machine. *Proceedings of the 2nd International Conference on New Forming Technology*, p. 135-144.

[8] Murata, M., Kato, T. (1999). Highly improved function and productivity for tube bending by CNC bender, from *http://www.tubenet.org.uk/technical/nissin.html*, accesed on 19-04-2011.

[9] Gantner, P., Bauer, H., Harrison, D.K., De Silva, A.K.M. (2005). Free-Bending - A new bending technique in the hydro forming process chain. *Journal of Materials Processing Technology*, vol. 167, p. 302-308, DOI:10.1016/j.jmatprotec.2005.05.052.

[10] Chatti, S., Hermes, M., Tekkaya, A.E., Kleiner, M. (2010). The new TSS bending process: 3D bending of profiles with arbitrary cross-sections. *CIRP Annals - Manufacturing Technology*, vol. 59, no. 1, p. 315-318, DOI:10.1016/j.cirp.2010.03.017.

[11] Chatti, S., Hermes, M., Kleiner, M. (2006). Three-dimensional-bending of profiles by stress superposition. *Advanced Methods in Material Forming*, Springer Verlag, p. 101-118.

[12] Staupendahl, D., Becker, C., Hermes, M., Tekkaya, A.E., Kleiner, M. (2011). New methods for manufacturing 3D-bent lightweight structures. *Proceedings of the 3rd International Conference on Steel in Cars and Trucks*, p. 120-129.

[13] Brosius, A., Hermes, M., Ben Khalifa, N., Trompeter, M., Tekkaya, A.E. (2009). Innovation by forming technology: motivation for research. *International Journal of Material Forming*, vol. 2, p. 29-38, DOI:10.1007/s12289-009-0656-9.

[14] El Megharbel, A., El Nasser, G.A., El Domiaty, A. (2007). Bending of tube and section made of strain-

hardening materials. *Journal of Materials Processing Technology*, vol. 203, p. 372-380, DOI:10.1016/j.jmatprotec.2007.10.078.

[15] Welo, T., Paulsen, F., Brobak, T.J. (1994). The behaviour of thin-walled Aluminium alloy profiles in rotary draw bending – a comparison between numerical and experimental results. *Journal of Materials Processing Technology*, vol. 45, no. 1-4, p. 173-180, DOI:10.1016/0924-0136(94)90337-9.

[16] Paulsen, F., Welo, T. (2002). A design method for prediction formed in stretch bending. *Journal of Materials Technology*, vol. 128, p. 48-66, DOI:10.1016/S0924-0136(02)00178-4.

[17] Zhao, G.Y., Liu, Y.L., Dong, C.S., Yang, H., Fan, X.G. (2010). Analysis of wrinkling limit of rotary-draw bending process for thin-walled rectangular tube. *Journal of Materials Processing Technology*, vol. 210, no. 9, p. 1224-1231, DOI:10.1016/j.jmatprotec.2010.03.009.

[18] Li, H., Yang, H., Zhan, M., Kou, Y.L. (2010). Deformation behaviours of thin-walled tube in rotary draw bending under push assistant loading conditions. *Journal of Materials Processing Technology*, vol. 210, p. 143-158, DOI:10.1016/j.jmatprotec.2009.07.024.

[19] Zhao, G.Y., Liu, Y.L., Yang, H., Lu, C.H. (2010). Cross-sectional distortion behaviours of thin-walled rectangular tube in rotary-draw bending process. *Transactions of Nonferrous Metals Society of China*, vol. 20, no. 3, p. 484-489, DOI:10.1016/S1003-6326(09)60166-7.

[20] Hermes, M., Kleiner, M. (2008). *Vorrichtung zum Profilbiegen (device for profile bending)*. German Patent Application, DE102007013902A1, Registr. Date 20.03.2007, München.

[21] Quareshi, H.A. (1999). Elastic-plastic analysis of tube bending. *International Journal of Machine Tools & Manufacture*, vol. 39, p. 87-104, DOI:10.1016/S0890-6955(98)00012-1.

[22] Tang, N.C. (2000). Plastic-deformation analysis in tube bending. *International Journal of Pressure Vessels and Piping*, vol. 77, p. 751-759, DOI:10.1016/S0308-0161(00)00061-2.

[23] Yang, H., Yan, J., Zhan, M., Li, H., Kou, Y. (2009). 3D numerical study on wrinkling characteristics in NC bending of aluminium alloy thin-walled tubes with large diameters under multi-die constraints. *Computational Materials Science*, vol. 45, p. 1052-1067, DOI:10.1016/j.commatsci.2009.01.010.

[24] Aimin, Y., Rongqiang, Y., Ying, H. (2009). Theory and application of naturally curved and twisted beams with closed thin walled cross sections. *Strojniški vestnik - Journal of Mechanical Engineering*, vol. 55, no. 12, p. 733-741.

[25] DIN EN 10305-1–MW1000L, Precision Tubes acc. For highly stressed components, Salzgitter Mannesmann Precision GmbH technical data sheet 049 R. (2009) (Werkstoffblatt 049 R).

[26] Shariati, M., Sedighi, M., Saemi, J., Allahbakhsh, H.R. (2010). A numerical and experimental study on buckling of cylindrical panels subjected to compressive axial load. *Strojniški vestnik - Journal of Mechanical Engineering*, vol. 56, no. 10, p. 609-618.

[27] Nițu, E., Iordache, M., Marincei, L., Charpentier, I., Le Coz, G., Ferron, G., Ungureanu, I. (2011). FE-Modeling of cold rolling by in-feed method of circular grooves. *Strojniški vestnik - Journal of Mechanical Engineering*, vol. 57, no. 9, p. 667-673, DOI:10.5545/sv-jme.2010.244.